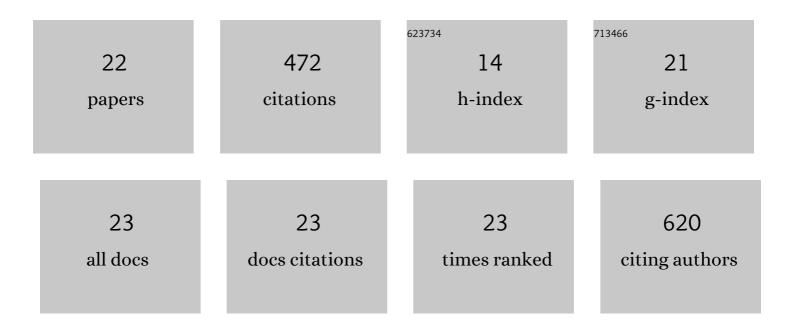
## Christopher T Winkelmann

List of Publications by Year in descending order

Source: https://exaly.com/author-pdf/11798307/publications.pdf Version: 2024-02-01



#	Article	IF	CITATIONS
1	InÂVivo Small Animal Imaging: A Comparison to Gross and Histopathologic Observations in Animal Models. , 2022, , 423-457.		0
2	fMRI study of the role of glutamate NMDA receptor in the olfactory processing in monkeys. PLoS ONE, 2018, 13, e0198395.	2.5	8
3	fMRI study of the role of glutamate NMDA receptor in the olfactory adaptation in rats: Insights into cellular and molecular mechanisms of olfactory adaptation. NeuroImage, 2017, 149, 348-360.	4.2	10
4	Assessment of near-infrared fluorophores to study the biodistribution and tumor targeting of an IL13 receptor α2 antibody by fluorescence molecular tomography. Oncotarget, 2017, 8, 57231-57245.	1.8	7
5	Odanacatib, effects of 16-month treatment and discontinuation of therapy on bone mass, turnover and strength in the ovariectomized rabbit model of osteopenia. Bone, 2016, 93, 86-96.	2.9	14
6	fMRI study of olfaction in the olfactory bulb and high olfactory structures of rats: Insight into their roles in habituation. Neurolmage, 2016, 127, 445-455.	4.2	23
7	Functional imaging of olfaction by CBV fMRI in monkeys: Insight into the role of olfactory bulb in habituation. NeuroImage, 2015, 106, 364-372.	4.2	24
8	Considerations for conducting imaging studies in support of developmental toxicology studies for regulatory submission. Reproductive Toxicology, 2014, 48, 41-43.	2.9	3
9	Effect of odanacatib on bone turnover markers, bone density and geometry of the spine and hip of ovariectomized monkeys: A head-to-head comparison with alendronate. Bone, 2013, 56, 489-496.	2.9	36
10	High-resolution peripheral quantitative computed tomography and finite element analysis of bone strength at the distal radius in ovariectomized adult rhesus monkey demonstrate efficacy of odanacatib and differentiation from alendronate. Bone, 2013, 56, 497-505.	2.9	34
11	In Vivo Small Animal Imaging. , 2013, , 287-315.		2
12	Micro omputed tomography imaging and analysis in developmental biology and toxicology. Birth Defects Research Part C: Embryo Today Reviews, 2013, 99, 71-82.	3.6	25
13	Non-invasive MicroCT Imaging Characterization and In Vivo Targeting of BB2 Receptor Expression of a PC-3 Bone Metastasis Model. Molecular Imaging and Biology, 2012, 14, 667-675.	2.6	10
14	Evaluation of high-resolution peripheral quantitative computed tomography, finite element analysis and biomechanical testing in a pre-clinical model of osteoporosis: A study with odanacatib treatment in the ovariectomized adult rhesus monkey. Bone, 2012, 50, 1379-1388.	2.9	30
15	Continuing Education Course #1. Toxicologic Pathology, 2011, 39, 267-272.	1.8	6
16	Microâ€computed tomographic evaluation of fetal skeletal changes induced by allâ€ <i>trans</i> â€retinoic acid in rats and rabbits. Birth Defects Research Part B: Developmental and Reproductive Toxicology, 2010, 89, 408-417.	1.4	25
17	High-throughput micro-computed tomography imaging as a method to evaluate rat and rabbit fetal skeletal abnormalities for developmental toxicity studies. Journal of Pharmacological and Toxicological Methods, 2009, 59, 156-165.	0.7	48
18	Microâ€computed tomography and alizarin red evaluations of boric acid–induced fetal skeletal changes in Spragueâ€Dawley rats. Birth Defects Research Part B: Developmental and Reproductive Toxicology, 2009, 86, 214-219.	1.4	27

#	Article	IF	CITATIONS
19	Evaluation of hydroxyurea-induced fetal skeletal changes in Dutch belted rabbits by micro-computed tomography and alizarin red staining. Birth Defects Research Part B: Developmental and Reproductive Toxicology, 2009, 86, 220-226.	1.4	27
20	TLD assessment of mouse dosimetry during microCT imaging. Medical Physics, 2008, 35, 3866-3874.	3.0	42
21	Microimaging Characterization of a B16-F10 Melanoma Metastasis Mouse Model. Molecular Imaging, 2006, 5, 7290.2006.00011.	1.4	39
22	Microimaging characterization of a B16-F10 melanoma metastasis mouse model. Molecular Imaging, 2006, 5, 105-14.	1.4	20